Lithos 332–333 (2019) 328–339

Contents lists available at ScienceDirect

Lithos

journal homepage: www.elsevier.com/locate/lithos

The origin and geodynamic significance of the Mesozoic dykes in eastern continental China

Juanjuan Kong [a,b,c,*], Yaoling Niu [a,b,d,e,*], Pu Sun [a,b], Yuanyuan Xiao [a,b], Pengyuan Guo [a,b], Di Hong [a,b,c], Yu Zhang [b], Fengli Shao [f], Xiaohong Wang [a,b], Meng Duan [a,e]

[a] Institute of Oceanology, Chinese Academy of Sciences, Qingdao 266071, China
[b] Laboratory for Marine Geology, Qingdao National Laboratory for Marine Science and Technology, Qingdao 266061, China
[c] University of Chinese Academy of Sciences, Beijing 100049, China
[d] Department of Earth Sciences, Durham University, Durham DH1 3LE, UK
[e] China University of Geosciences, Beijing 100083, China
[f] Linyi University, Linyi 276000, China

ARTICLE INFO

Article history:
Received 20 September 2018
Accepted 27 February 2019
Available online 06 March 2019

Keywords:
Dykes
Petrogenesis
Subduction of the paleo-pacific plate
Metasomatized lithospheric mantle
Eastern China

ABSTRACT

We sampled 22 Mesozoic dykes in eastern continental China and carried out a detailed study on these samples, including K–Ar and zircon U–Pb geochronology, and elemental and Sr-Nd-Pb-Hf isotope geochemistry. Their K–Ar and zircon ages of 130-110 Ma are broadly consistent with the timing of the lithosphere thinning and the emplacement ages of widespread granitoids in the vast region, explicitly pointing to a common cause in space and time. The dykes represent evolved alkaline basaltic melts intruding the Mesozoic granitoids. Their rare earth element (REE) and multi-element patterns differ from the present-day ocean island basalts (OIB), but show strong arc-like signatures (e.g., enrichment in Rb and Pb and depletion in Nb, Ta and Ti). They show high $(^{87}Sr/^{86}Sr)_i$ (0.7048 to 0.7103), low $\varepsilon_{Nd}(t)$ (−12.3 to −5.7), low $\varepsilon_{Hf}(t)$ (−16.5 to −8.0) and low $(^{206}Pb/^{204}Pb)_i$ (18.79–18.85). These Mesozoic dykes are best understood as resulting from melting of geochemically enriched subcontinental lithospheric mantle (SCLM), whose geochemical enrichment is consistent with prior metasomatism with the agent being hydrous melt coming from subduction of the Paleo-Pacific plate at ~120 Ma or earlier. Similar to the present-day situation, the paleo-Pacific slab may have also existed stagnant in the mantle transition zone in the Mesozoic. The slab dehydrated and released water in the form of hydrous melt that percolated through and metasomatized the mantle lithosphere, and weakened the base of the lithosphere while producing basaltic melts that evolved to intermediate-felsic compositions of these dykes. The basaltic magmas that underplated and melted the lower crust to generate the widespread Mesozoic granitoids in eastern continental China.

1. Introduction

The Paleozoic diamondiferous kimberlite volcanism in eastern continental China indicates the existence of a long-lived craton such as the North China Craton (NCC) with the lithosphere thickness in excess of 200 km. However, the present-day lithosphere thickness of 60–80 km beneath the vast region and the widespread magmatic activities in the Mesozoic and since then point to the lithospheric destructions since the Mesozoic (e.g., Wong, 1929; Menzies et al., 1993; Griffin et al., 1998; Zheng et al., 1998; Gao et al., 2002; Zhou et al., 2002; Wu et al., 2003; Yang et al., 2003; Zhang et al., 2004; Zhu et al., 2012; Niu, 2014). However, the exact mechanisms of the lithospheric destruction remain speculative. Principal mechanisms proposed include delamination (e.g., Deng et al., 2007; Gao et al., 2004; Li et al., 2012; Lin and Wang, 2006; Liu et al., 2008a, 2008b; Windley et al., 2010; Wu et al., 2005; Xu et al., 2008; Xu et al., 2013), thermo-chemical erosion (e.g., Fan and Menzies, 1992; Griffin et al., 1998; Menzies et al., 1993; Xu et al., 2004; Xu et al., 2009; Zheng et al., 1998; Zheng et al., 2006, 2007), basal hydration-weakening (Niu, 2005, 2014; Niu et al., 2015) and flat subduction (Wu et al., 2017). Different opinions may still exist, but the effect of paleo Pacific plate subduction is now widely accepted. For example, the lithosphere thinning accompanied by the widespread volcanism during the Mesozoic is interpreted to be genetically related to dehydration of such a subducted slab in the mantle transition zone (Guo et al., 2014; Niu, 2005, 2014; Niu et al., 2015; Xu, 2014; Xu et al., 2012; Zhu et al., 2012). Multiple lines of evidence suggest that subduction of the paleo Pacific plate strongly influenced geological processes in eastern continental China since the Mesozoic (Guo et al., 2014; Niu, 2005; Niu et al., 2015; Wang et al., 2015; Wu et al., 2005; Zhou and

* Corresponding authors at: Institute of Oceanology, Chinese Academy of Sciences, Qingdao 266071, China.
E-mail addresses: juanjuan0317@foxmail.com (J. Kong), yaoling.niu@durham.ac.uk (Y. Niu).

https://doi.org/10.1016/j.lithos.2019.02.024
0024-4937/

Li, 2000; Zhu et al., 2012). Therefore, it is imperative to objectively evaluate whether melts from the subducted Paleo Pacific plate may have contributed to the widespread Mesozoic magmatism in eastern continental China.

The mantle-derived mafic rocks in the Mesozoic have been interpreted to be genetically related to the lithospheric thinning (e.g., Niu, 2005; Xu, 2014), and study of these rocks can help explore the timing and mechanism of lithospheric thinning. The Mesozoic mafic dykes are widespread in eastern continental China, and mainly striking NW-SE and intruding Mesozoic granitoids and old basement rocks (Dai et al., 2016; Liang et al., 2016). The concept of basal hydration weakening that thinned the mantle lithosphere in eastern continental China (Niu, 2005, 2014) assumed that the Cretaceous mafic magmatic rocks, including the dykes we study here, resulted from melting the thinning mantle lithosphere. One of our current research objectives in the region is to test the validity of this assumption. In this paper, we present our testing result through studying the major element, trace element and Sr-Nd-Pb-Hf isotope compositions of representative Cretaceous dykes from eastern continental China.

2. Geology and samples

The eastern continental China includes the Northeast (NE) China, North China Craton (NCC), the Dabie Orogen, and the South China Cratons (SCC) (Fig. 1). NE China is located in the eastern segment of the Central Asian Orogenic Belt and is generally considered to be a tectonic collage of several microcontinental blocks (Jahn et al., 2000a, 2000b, 2004; Li et al., 2013; Windley et al., 2007). The NCC is one of the oldest cratons in the world with an oldest zircon age record of >3.8 Ga (Liu et al., 1992), consisting of the eastern and western Archean blocks separated by the 1.8 Ga Proterozoic orogenic belt (Zhao et al., 2001; Fig. 1).

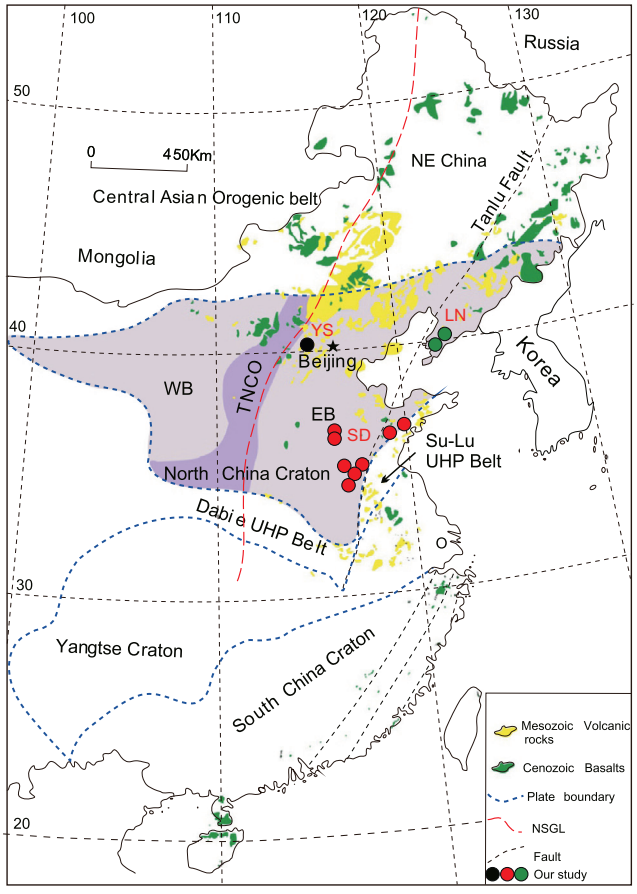

Fig. 1. (a) Sketch map of major tectonic divisions of the eastern continental China and the distribution of the Mesozoic dykes. WB, TNCO and EB denote three divisions of the North China Craton into the Western Block, Trans-North China Orogen and Eastern Block, respectively (Zhao et al., 2001). NSGL indicates the North-South Gravity Lineament. Modified after Guo et al. (2014).

We collected fresh and representative Cretaceous dykes from the north and northeast China, including diabases, gabbros and diorite. The dykes intruding the granitoids are well exposed (Fig. 2). The sampled dykes run NNE, and the dyke thicknesses vary from 0.2 to 1.5 m (Fig. 2). The sample details are given in Appendix A. The dyke rocks collected in the Shandong area (SD in Fig. 1) are deep green. These dykes are fresh and porphyritic with ~10% olivine phenocrysts. The gabbros consist of 25% coarse grained phenocrysts of clinopyroxene and plagioclase, and 75% matrix of clinopyroxene, plagioclase, magnetite and minor biotite (Fig. 3a, b). Diorite of DBZ-45 (also collected in the Shandong area) mainly consists of plagioclase (40–50%) and hornblende (30–45%). The dykes collected in the Yanshan area (YS in Fig. 1) are fresh and porphyritic, consisting of plagioclase (40–50%), clinopyroxene (30–40%), varying amount of biotite and hornblende (1–5%), and minor disseminated magnetite (5%; Fig. 3c, d). With a holocrystalline/diabasic texture, the dykes from the Liaoning area (LN in Fig. 1) are made up of quench microlites of plagioclase, pyroxene, olivine and opaques with olivine phenocryst occasionally seen (Fig. 3e, f).

3. Analytical methods

3.1. K–Ar

Fresh basaltic samples were selected for dating. They were crushed into ~1 mm grains and washed in distilled water. Conventional whole-rock K–Ar dating was carried out at Key Laboratory of Orogenic Belts and Crustal Evolution at Peking University for five samples. We analyzed Ar isotopes in a VSS-RGA-10 mass spectrometer (1986). The data were corrected for mass discrimination, nucleogenic interferences, and atmospheric contamination following the procedures in K–Ar Data Processing 1.0. A K–Ar age value of ZBH-25 (biotite of granodiorite in Fangshan) is 132.47 Ma (Recommended value is 132.9 ± 1.3 Ma) for atmospheric argon, which is used for the calculation of the mass spectrometer discrimination (Sang et al., 2006).

3.2. Zircon U–Pb

Zircons from five samples were separated for U–Pb dating using methods of heavy magnetic techniques. Cathodoluminescence (CL) imaging was carried out using a CL spectrometer (Gatan Mini CL) equipped on a Jeol 6510 scanning electron microscope (SEM) at the Beijing GeoAnalysis Co., Ltd. U–Pb dating was conducted using laser ablation inductively coupled plasma mass spectrometry (LA-ICP-MS) at the Institute of Oceanology, Chinese Academy of Sciences (IOCAS), Qingdao. Zircons were ablated with a 193 nm excimer laser system produced by Photon-Machines company. Using a 25 μm spot size, frequency of 4 Hz and intensity of 100% (Xiao et al., under review). Zircon 91,500 was used as external standard. Off-line selection and integration of background and analyte signals, and time-drift correction and quantitative calibration for trace element analyses and U–Pb dating were performed by ICP-MS-Data-Cal (Liu et al., 2010a; Liu et al., 2010b). Concordia diagrams and weighted mean age calculations were processed using Isoplot/Ex-version 4.15 (Ludwig, 2012).

3.3. Major and trace elements

We chose freshest samples for geochemical analysis. After the weathered surfaces, pen marks and saw marks were removed, the sample chips were thoroughly cleaned ultrasonically with Milli-Q water, dried and then powdered using an agate mill in a clean environment.

Whole-rock major and trace elements were analyzed at IOCAS, using an Agilent-5100 inductively coupled plasma-optical emission spectrometer (ICP-OES) and Agilent-7900 inductively coupled plasma

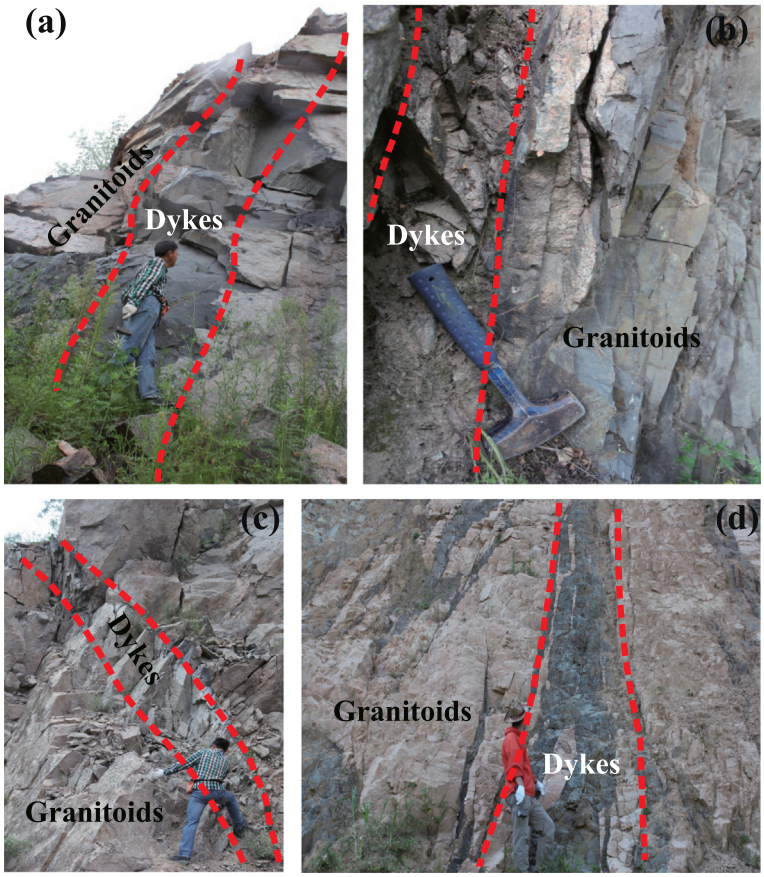

Fig. 2. Outcrop of the Cretaceous dykes in eastern China.

mass spectrometer (ICP-MS), respectively. For major elements, ~50 mg sample powder was placed in a platinum crucible and melted at 1050 °C for 1 h in a muffle furnace. Then, the crucible was further heated over a Bunsen burner (Dragon series) at 1000 °C to ensure all sample materials forming a single coherent melt drop that was finally poured/quenched into ~50 mL 5% HNO_3 solution at room temperature. The solution was then diluted into 100 mL with Milli-Q water in clean plastic bottle for analysis. The analytical details are given in Appendix B. The ICP-OES analytical precision is better than 5% (RSD, relative standard deviation; see Appendix C for details). The values of USGS reference materials BCR-2, STM-2 and W-2 run with our samples are given in Appendix D, which are consistent with the reported reference values. For loss on ignition (LOI) analysis, ~500 mg samples were weighed and heated in a muffle furnace at 950 °C for 2 h, cooled in a desiccator, and then weighed again to calculate the weight loss as the LOI.

For trace element analysis, fifty milligram powder of each sample was dissolved with acid mix (1:1) of distilled HF and HNO_3 in a high pressure jacket equipped Teflon beaker till complete digestion/dissolution. Analytical precision is better than 5% for most elements. During trace element analysis, USGS reference materials AGV-2 and BCR-2 were used to monitor the analytical accuracy and precision. The values of AGV-2 and BCR-2 run with our samples are given in Appendix E, which are consistent with the reported reference values. Sample digestion and analytical details are given in Chen et al. (2017).

3.4. Sr-Nd-Pb-Hf isotopes

Whole-rock Sr-Nd-Pb-Hf isotopic analyses were done in the Radiogenic Isotope Facility at the University of Queensland, Australia. The rock powders were dissolved in a mixture of double-distilled concentrate HNO_3 and HF, and dried on a hot plate at 80 °C. After converting any fluoride to nitrate, the dried residue was dissolved with 3 mL 2 N HNO_3. 1.5 mL sample solution was loaded onto a stack of Sr-spec, Thru-spec and LN-spec resin columns to separate Sr, Pb, Nd and Hf, using a streamlined procedure modified after Míková and Denková (2007) and Yang et al. (2010). The measurement of $^{87}Sr/^{86}Sr$, $^{143}Nd/^{144}Nd$ and $^{176}Hf/^{177}Hf$ ratios was conducted in static mode on a Nu Plasma HR MC-ICP-MS using a modified CETAC ASX-110FR autosampler and a DSN-100 dissolvation nebulizing system. All measured $^{87}Sr/^{86}Sr$, $^{143}Nd/^{144}Nd$ and $^{176}Hf/^{177}Hf$ ratios were normalized to $^{86}Sr/^{88}Sr = 0.1194$, $^{146}Nd/^{144}Nd = 0.7219$ and $^{179}Hf/^{177}Hf = 0.7325$, respectively. Analyses of NBS987 standard run during the same period gave $^{87}Sr/^{86}Sr = 0.710249 \pm 17$ ($n = 18$, 2σ). In the course of $^{143}Nd/^{144}Nd$ and $^{176}Hf/^{177}Hf$ analysis, the in-house Nd standard, Ames Nd Metal and 10 ppm Hf ICP solution from Choice Analytical were used as instrument drift monitors, respectively. This in-house Nd Metal and Hf standards were cross-calibrated against the JNdi-1 Nd international standard and the JMC-475 Hf international standard, respectively. Analyses of in-house Nd standard gave $^{143}Nd/^{144}Nd = 0.511966 \pm 12$ ($n = 24$, 2σ), corresponding to a mean value of 0.282160 ± 6 ($n = 16$, 2σ) for JNdi-1 standard. Analyses of in house Hf standard yielded a mean $^{176}Hf/^{177}Hf$ of 0.282146 ± 12 ($n = 31$, 2σ). The values of USGS reference materials JG-3 and BCR-2 run with our samples are given in Appendix F, which are consistent with the reported reference values. Analytical details are given in Guo et al. (2014).

4. Results

4.1. K–Ar dating

Our K–Ar dating on representative samples (Appendix G) give emplacement ages of 132.5-120.0 Ma for these dykes.

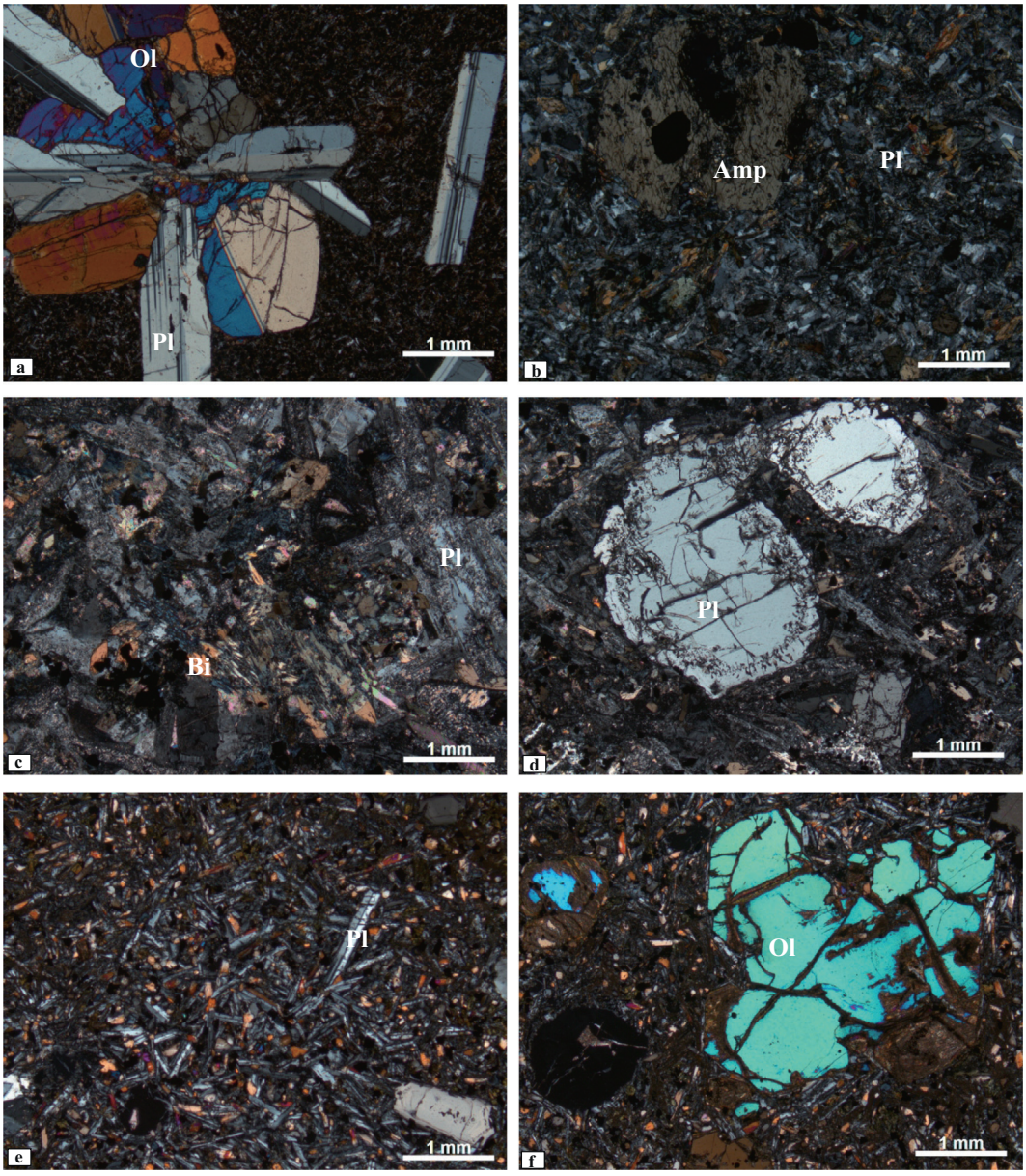

Fig. 3. Photomicrographs of representative dykes. (a) Sample SD14-32, XPL; (b) sample SD14-71, XPL; (c) sample YS14-31, XPL; (d) sample YS14-33, XPL; (e) sample LN14-40, XPL and (f) sample LN14-40, PPL. Cpx-clinopyroxene; Pl-plagioclase; Bt-biotite; Ol-olivine.

4.2. Zircon U–Pb ages

Representative CL images of analyzed zircons and corresponding concordia diagrams are shown in Fig. 4. The age data are given in Appendix H.

Zircons from dyke samples are pale green, euhedral columnar crystals (80–150 μm long) with aspect ratios of ~1.5:1–2:1 (Fig. 4). The LA-ICP-MS U–Pb analysis gave variable Th (242–2508 ppm) and U (658–7565 ppm) concentrations with Th/U ratios of 0.25–0.67 (Appendix H), which are consistent with a magmatic origin (Belousova et al., 2002; Hoskin and Schaltegger, 2003). Thus, the youngest U–Pb age group of the zircons represents the crystallization age. The measured $^{206}Pb/^{238}U$ ages for the five dyke samples are identical, yielding a weighted mean age of 128.0 ± 3.1 Ma (1σ, MSWD = 1.9, n = 6) for sample LN14-32, 120 ± 15 Ma (1σ, MSWD = 19, n = 4) for sample SD14-30, 115.9 ± 2.4 Ma (1σ, MSWD = 2.2, n = 9) for sample SD14-33, 109.1 ± 2.6 Ma (1σ, MSWD = 1.4, n = 7) for SD14–38, and 126.1 ± 1.4 Ma (1σ, MSWD = 1.5, n = 10) for DBZ15-47, respectively (Fig. 4). The high MSWD up to 19 while calculating the weighted mean age of sample SD14-30 was resulted from the facts that the zircon grains are few in quantity and very small in size, the core of the zircon was hit during analysis (Fig. 4b). These ages are taken to represent the intrusive age of the dykes. And the ages of other samples are list in Appendix A.

4.3. Major elements

Whole-rock major and trace elements are given in Table 1.

The dykes from the eastern China plot in the fields of basaltic trachyandesite and trachybasalt on the total alkali-silica (TAS) diagram (Fig. 5). The dykes represent variably evolved melts characterized by moderate silica (45.76–63.04 wt%), high Al_2O_3 (13.00–17.50 wt%) and low $Mg^{\#}$ (0.47–0.54) ($Mg^{\#}$ = molar Mg/[Mg + Fe^{2+}]). In MgO variation diagrams, the data define scattered yet linear and more or less continuous trends (SiO_2, Al_2O_3, CaO, CaO/Al_2O_3, Cr and Ni, Fig. 6). There are random correlations of MgO vs. TiO_2, Fe_2O_3 and P_2O_5.

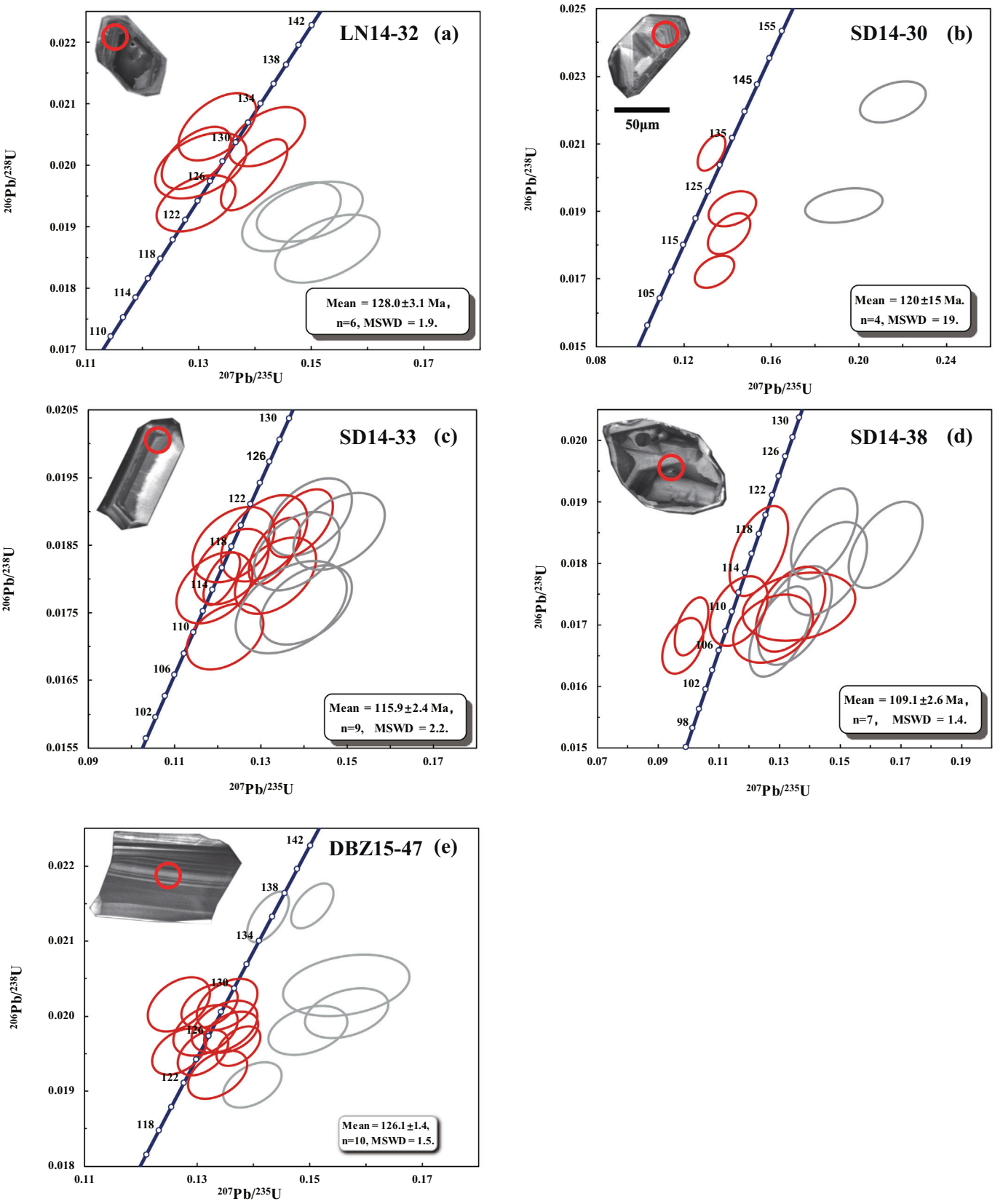

Fig. 4. Concordia diagrams of dated zircons from sample (a) LN14-32 (diabase), (b) SD14-30 (gabbro), (c) SD14-33 (gabbro), (d) SD14-38 (gabbro) and (e) DBZ15-47 (diorite) of the Cretaceous dykes. The weighted mean $^{206}Pb/^{238}U$ age corresponds to the red circle analyses. (For interpretation of the references to colour in this figure legend, the reader is referred to the web version of this article.)

Table 1
Major and trace elements composition of the dykes in eastern China.

	DBZ15-44	DBZ15-45	DBZ15-46	DBZ15-47	LN14-32	LN14-45	SD14-16	SD14-30	SD14-32	SD14-36	SD14-37	SD14-38	SD14-43	SD14-64	SD14-71	XJZZ11-04	XJZZ11-06	YS14-27	YS14-31	YS14-32	YS14-33	YS14-37	DBZ14-46^{REP}
Major element (wt%)																							
SiO_2	54.31	55.01	53.70	55.29	51.73	48.12	55.46	53.65	48.93	51.82	47.56	54.01	61.73	51.04	63.04	50.33	50.97	50.40	47.92	55.42	48.76	45.76	53.66
TiO_2	0.78	0.86	0.83	0.90	0.99	1.11	0.87	0.94	2.40	1.20	1.35	1.21	0.81	1.44	0.78	0.89	0.98	1.98	2.10	1.26	1.82	2.20	0.82
Al_2O_3	14.03	15.00	14.42	15.41	15.48	15.22	17.50	14.40	15.38	15.78	15.83	17.26	15.01	15.46	15.66	7.89	13.00	17.26	16.04	15.44	15.72	14.09	14.69
TFe_2O_3	9.45	9.20	8.88	8.57	8.63	8.08	6.53	5.71	11.73	8.12	8.04	7.42	5.48	8.16	5.87	9.72	8.13	9.86	11.25	6.43	10.10	12.29	9.04
CaO	7.92	7.08	7.55	6.97	7.37	7.17	5.76	5.07	8.55	7.77	8.37	4.38	4.69	6.30	4.33	11.61	10.02	5.02	6.57	4.95	7.50	8.18	7.57
MnO_2	0.147	0.116	0.137	0.134	0.126	0.123	0.195	0.091	0.275	0.203	0.154	0.283	0.158	0.140	0.082	0.155	0.124	0.121	0.147	0.083	0.126	0.161	0.140
MgO	7.8	4.71	5.87	4.48	7.96	6.63	4.12	4.53	5.01	7.80	6.29	5.90	3.69	7.31	3.07	14.74	9.20	3.54	5.87	3.20	5.66	7.45	5.99
Na_2O	3.18	3.38	3.09	3.66	3.88	2.96	4.76	3.45	3.55	3.12	3.10	3.91	3.45	3.95	3.86	1.41	3.01	5.06	4.18	4.77	3.45	3.48	3.16
K_2O	2.23	2.48	2.5	2.18	1.78	2.47	3.33	3.10	1.44	3.15	2.77	4.61	3.68	2.71	4.22	1.91	2.09	3.14	1.80	2.07	2.98	2.00	2.40
P_2O_5	0.35	0.36	0.32	0.38	0.25	0.47	0.44	0.56	0.55	0.57	0.91	0.60	0.45	0.48	0.48	0.24	0.73	1.25	0.69	0.54	0.93	1.11	0.33
LOI	0.64	3.12	2.92	2.68	5.15	5.61	1.30	8.45	4.33	1.08	7.66	2.73	1.16	2.92	1.24	2.37	2.57	3.72	3.93	5.16	4.01	3.49	2.92
Total	100.83	101.32	100.21	100.65	103.35	97.96	100.26	99.95	102.14	100.61	102.04	102.31	100.31	99.91	102.64	101.27	100.82	101.35	100.50	99.33	101.06	100.21	100.72
CaO/Al_2O_3	0.56	0.47	0.52	0.45	0.48	0.47	0.33	0.35	0.56	0.49	0.53	0.25	0.31	0.41	0.28	1.47	0.77	0.29	0.41	0.32	0.48	0.58	0.46
Trace element (ppm)																							SD14-16^{REP}
Sc	26.6	24.0	26.2	22.3	25.4	20.2	12.9	15.9	18.5	20.5	17.0	18.7	12.7	21.1	12.3	33.8	21.7	10.4	17.7	10.2	18.8	20.2	12.1
V	207	208	227	206	182	184	119	121	231	172	147	144	97	168	105	171	166	151	207	117	189	234	131
Cr	380	104	206	62.8	399	319	25.2	148	40.9	277	207	309	106	280	92.0	786	446	2.91	88	63.7	107	279	31.9
Co	34.1	21.5	29.9	22.4	33.5	29.1	10.0	18.9	32.0	29.6	28.2	25.2	14.1	33.0	15.5	47.1	34.6	22.2	28.3	15.3	28.9	42.5	10.8
Ni	101.7	26.4	61.9	16.6	70.2	132	10.2	57.0	59.0	134	126	104	50.5	127.7	32.3	288	175	8.91	43.7	32.3	56.5	119	10.7
Rb	46.8	86.9	71.3	41.4	57.7	49.0	117	73.8	25.5	106	51.8	209	146	87.8	64.3	48.8	41.6	63.7	31.1	41.6	69.9	36.0	120
Sr	704	674	594	739	436	778	890	560	501	965	1069	1031	845	890	619	533	1501	1248	962	1150	1569	1396	907
Y	14.0	16.7	16.4	16.4	15.7	18.5	20.6	18.7	26.4	19.6	23.0	31.9	25.2	20.7	22.7	17.8	20.8	20.6	20.9	12.5	19.4	16.9	20.9
Zr	89.9	114	120	119	117	160	221	207	206	204	253	192	314	246	220	188	151	267	203	216	230	175	231
Nb	4.09	5.23	5.80	5.66	5.89	8.62	10.4	12.6	29.9	15.6	21.1	22.0	15.1	10.6	23.0	9.49	8.32	31.2	30.5	10.2	22.0	20.5	10.4
Ba	787	758	836	919	507	926	2032	2588	512	1844	2092	2187	2326	1789	1374	1005	1633	1646	1056	1415	1935	1103	1902
La	18.5	17.1	24.2	21.7	24.1	41.7	43.5	43.0	29.1	41.8	59.2	46.5	73.6	71.1	41.3	52.0	102	68.9	50.1	50.3	56.4	52.0	60.5
Ce	39.5	38.8	49.5	46.4	47.9	82.8	93.7	85.3	59.6	82.3	119	90.4	138	138	80.6	113	201	146	105	103	117	115	117
Pr	4.96	5.09	5.95	5.76	5.73	9.77	11.4	10.1	7.37	9.66	14.2	10.5	15.4	15.6	9.39	14.0	23.8	17.8	12.8	12.6	14.2	14.3	13.2
Nd	20.8	22.1	24.1	23.9	22.5	38.0	43.5	38.8	30.4	37.2	53.3	39.4	54.5	56.2	36.2	55.4	90.5	64.7	48.2	47.4	53.7	54.5	46.9
Sm	4.15	4.74	4.81	4.68	4.20	6.75	7.52	7.20	6.73	6.48	9.03	6.83	8.88	9.24	6.56	9.48	13.00	9.70	7.85	7.68	8.76	8.33	7.54
Eu	1.26	1.48	1.32	1.40	1.38	1.99	1.99	2.05	2.26	2.00	2.65	2.04	2.19	2.31	1.99	2.04	3.30	2.71	2.28	2.16	2.51	2.46	2.03
Gd	3.60	4.24	4.22	4.14	3.93	5.21	5.69	5.90	6.75	5.49	7.14	6.26	6.73	6.78	5.90	6.68	8.49	6.84	6.17	5.23	6.71	6.11	5.67
Tb	0.52	0.60	0.59	0.58	0.55	0.70	0.74	0.76	0.99	0.74	0.93	0.93	0.93	0.89	0.85	0.81	1.01	0.88	0.83	0.64	0.83	0.76	0.77
Dy	2.67	3.17	3.06	3.03	3.01	3.55	3.89	3.72	5.26	3.77	4.54	5.09	4.77	4.22	4.35	3.87	4.44	4.22	4.19	2.76	4.01	3.59	3.91
Ho	0.55	0.66	0.64	0.64	0.63	0.70	0.81	0.73	1.05	0.78	0.90	1.13	0.97	0.83	0.90	0.72	0.80	0.83	0.84	0.50	0.76	0.68	0.82
Er	1.49	1.73	1.00	1.73	1.57	1.88	2.15	1.82	2.54	1.92	2.17	2.83	2.45	1.94	2.31	1.81	2.02	1.99	2.08	1.10	1.81	1.56	2.11
Tm	0.22	0.26	0.25	0.25	0.24	0.26	0.33	0.27	0.35	0.28	0.31	0.38	0.36	0.29	0.32	0.25	0.28	0.29	0.31	0.15	0.25	0.22	0.32
Yb	1.29	1.59	1.52	1.55	1.42	1.60	2.03	1.61	2.00	1.69	1.87	2.18	2.28	1.73	2.02	1.51	1.56	1.74	1.83	0.86	1.52	1.29	2.03
Lu	0.19	0.23	0.22	0.23	0.22	0.23	0.33	0.25	0.30	0.27	0.30	0.35	0.36	0.27	0.32	0.21	0.23	0.27	0.28	0.12	0.22	0.19	0.33
Hf	2.29	2.92	3.07	2.99	2.98	3.65	5.42	4.93	4.85	4.56	5.48	4.49	7.33	6.05	4.99	4.75	3.63	6.02	4.59	5.15	5.13	4.11	5.52
Ta	0.22	0.29	0.33	0.31	0.32	0.46	0.68	0.70	1.80	0.85	1.16	1.17	0.84	0.69	1.33	0.48	0.39	1.68	1.62	0.49	1.07	1.03	0.65
Pb	7.40	6.15	11.5	8.20	6.91	12.7	18.5	20.5	2.51	6.49	8.66	7.47	7.79	16.4	5.82	8.59	9.98	11.1	7.70	13.2	10.9	14.9	19.6
Th	1.91	3.64	5.29	2.18	3.29	4.64	13.3	4.15	3.12	3.97	4.81	4.11	8.76	14.7	3.72	10.5	7.15	3.16	3.04	4.80	3.19	2.15	13.1
U	0.60	1.26	1.50	0.65	0.66	0.96	2.96	8.98	0.85	0.98	1.09	2.29	2.08	2.48	1.42	1.70	1.30	0.87	0.84	1.24	0.77	0.70	2.84

REP: replicate sample. LOI is loss on ignition.

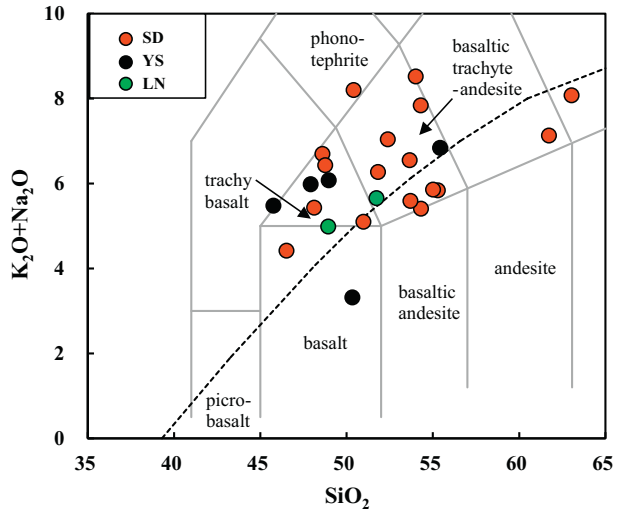

Fig. 5. The $K_2O + Na_2O$ vs. SiO_2 diagram showing compositions of the Cretaceous dykes. LN-dykes in Liaoning, YS-dykes in Yanshan, SD-dykes in Shandong.

4.4. Trace elements

The dykes show enrichment in light rare earth elements (LREEs) ($(La/Yb)N = 7.69$ to 46.85) and large ion lithophile elements (LILEs, such as Ba, Sr, Pb and K) without Eu anomalies (Fig. 7). These dykes show arc-like signature with negative HFSEs (such as Nb, Ta and Ti) anomalies (Fig. 7b), which are distinguished from average MORB and OIB (Sun and McDonough, 1989). These dykes have higher $[La/Sm]_N$ (2.3–5.1, primitive mantle normalized La/Sm) than average OIB (~2.4; Sun and McDonough, 1989), reflecting a highly enriched mantle source (Niu and Batiza, 1997). They show relatively large variations in Nb/U (1.41–36.22), Ce/Pb (4.16–20.18), Th/U (0.46–5.00, the low Th/U of 0.46 may due to being weathered) and Zr/Hf (38.95–44.82). These variations were found previously in intraplate basaltic rocks (Dupuy et al., 1992).

4.5. Whole rock Sr-Nd-Pb-Hf isotopes

The isotopic data are given in Appendix I. The initial isotopic ratios are calculated using zircon U–Pb ages of representative sample of this study (see above). The dykes have present-day $^{87}Sr/^{86}Sr$ of 0.7050 to 0.7110 (initial $^{87}Sr/^{86}Sr$ $[I_{Sr}] = 0.7048$ to 0.7103) (Fig. 8a). They display

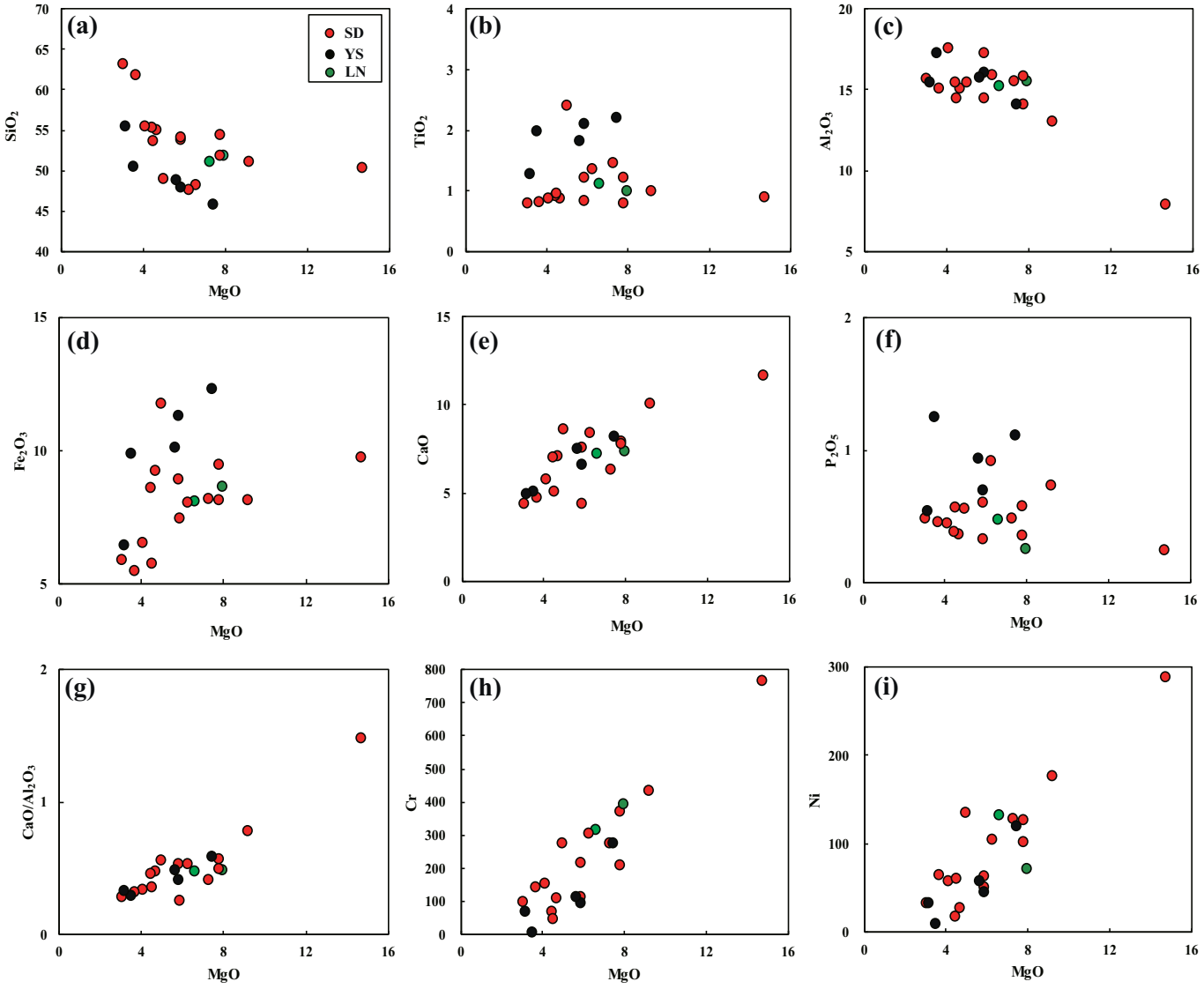

Fig. 6. MgO variation diagrams of the Cretaceous dykes. LN-dykes in Liaoning, YS-dykes in Yanshan, SD-dykes in Shandong.

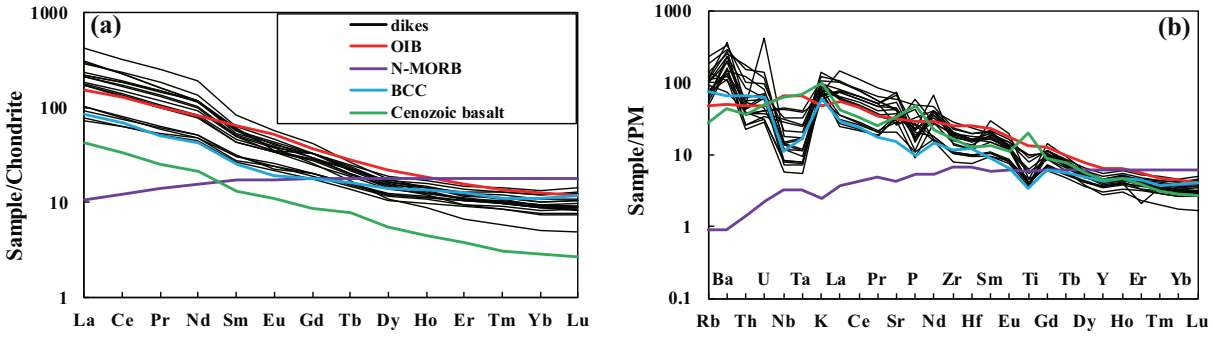

Fig. 7. (a) Chondrite-normalized rare earth element (REE) and (b) Primitive mantle (PM) normalized multi-element diagrams of the dykes. Average compositions of ocean island basalts (OIBs), bulk continental crust (BCC), and N-MORB, Cenozoic basalt compositions are also plotted for comparison. Chondrite, primitive mantle, N-MORB and OIB data are from Sun and McDonough (1989), BCC data are from Rudnick and Gao (2003). Cenozoic basalt data are from Sakuyama et al. (2013).

variably enriched Nd and Hf isotopic compositions ($\varepsilon_{Nd}(t = 120\ Ma) = -12.3$ to -5.7, $\varepsilon_{Hf}(t = 120\ Ma) = -16.5$ to -8.0) (Fig. 8b). The initial $^{206}Pb/^{204}Pb$, $^{207}Pb/^{204}Pb$ and $^{208}Pb/^{204}Pb$ ratios of the dykes are 18.79–18.85, 15.64–15.65 and 38.78–38.84, respectively (see below, Fig. 9). In the $^{208}Pb/^{204}Pb$ vs. $^{206}Pb/^{204}Pb$ plot (Fig. 9a), the scattered linear array is significantly displaced above the Northern Hemisphere Reference Line (NHRL), showing the Dupal signature (Hart, 1984). In the $^{207}Pb/^{204}Pb$ vs. $^{206}Pb/^{204}Pb$ diagram (Fig. 9b), the scattered data array plot displays an array above the NHRL. The Pb isotopic compositions are comparable to those of the Mesozoic mafic rocks from the North China Craton (Xie et al., 2006; Zhang et al., 2004) although more scattered with some samples plotting beyond the array (Figs. 8, 9), most likely resulting from mantle source heterogeneity on varying local scales because these samples are from a geographically large area (see in Fig. 1). The contemporaneous Mesozoic granitoids (gray dots in Fig. 9) in eastern continental China have similar Pb isotopic compositions to our dykes (Fig. 9).

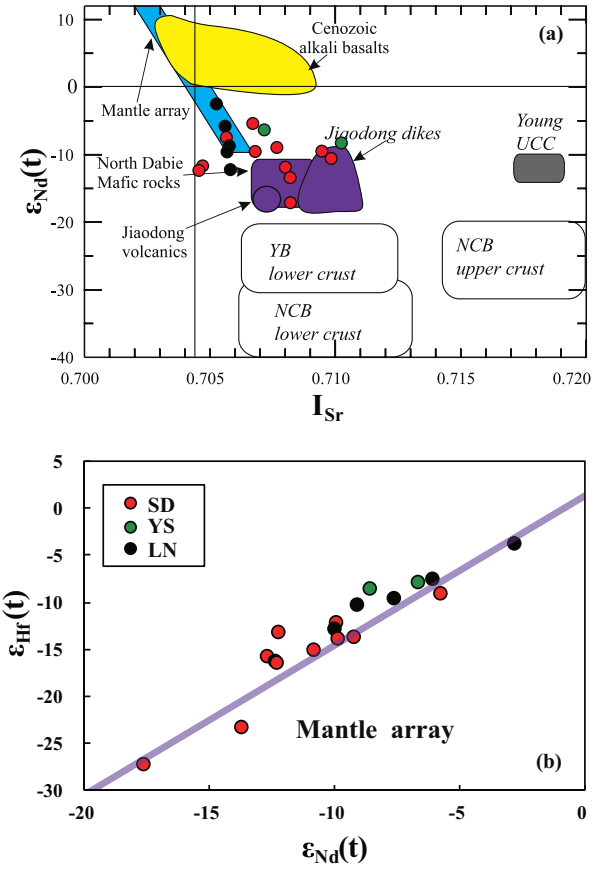

Fig. 8. (a) $\varepsilon_{Nd}(t = 120\ Ma)$ vs. initial $^{87}Sr/^{86}Sr$ and (b) $\varepsilon_{Hf}(t = 120\ Ma)$ vs. $\varepsilon_{Nd}(t = 120\ Ma)$ diagrams showing the dykes. The line for Hf–Nd mantle array is from Vervoort and Blichert-Toft (1999). LN-dykes in Liaoning, YS-dykes in Yanshan, SD-dykes in Shandong.

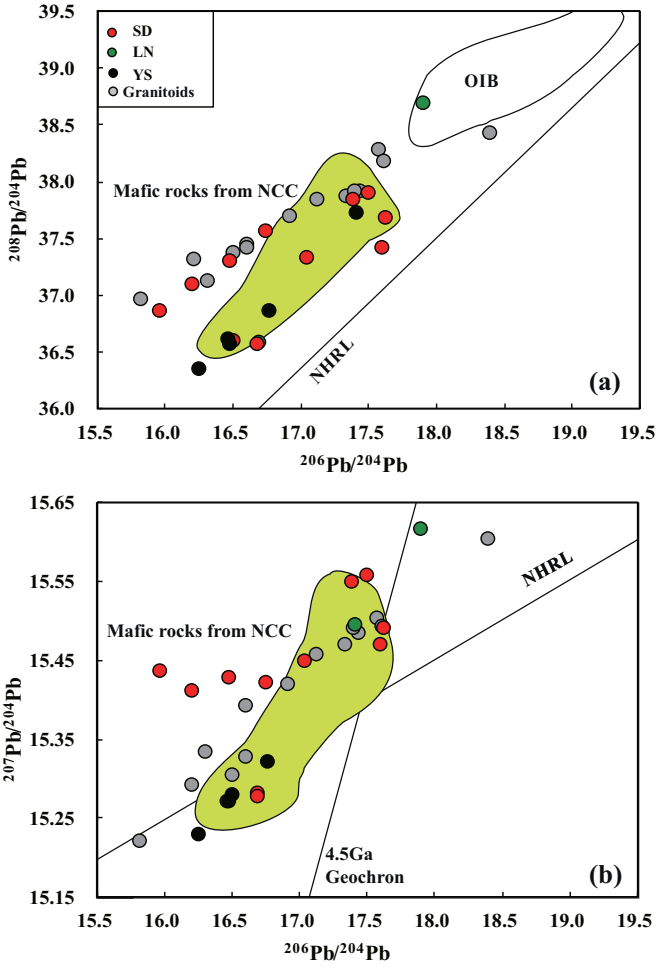

Fig. 9. Plots of $^{206}Pb/^{204}Pb$ vs. (a) $^{207}Pb/^{204}Pb$ and (b) $^{208}Pb/^{204}Pb$ ratios of the dykes. The NHRL and are from Barry and Kent (1988), Zou et al. (2000) and Hart (1984). NHRL: northern hemisphere reference line. The gray dots represent the contemporaneous granitoids of eastern China (Hong et al., 2018). ThePb isotopes of mafic rocks of North China craton are from Zhang et al. (2004) and Xie et al. (2006). LN-dykes in Liaoning, YS-dykes in Yanshan, SD-dykes in Shandong.

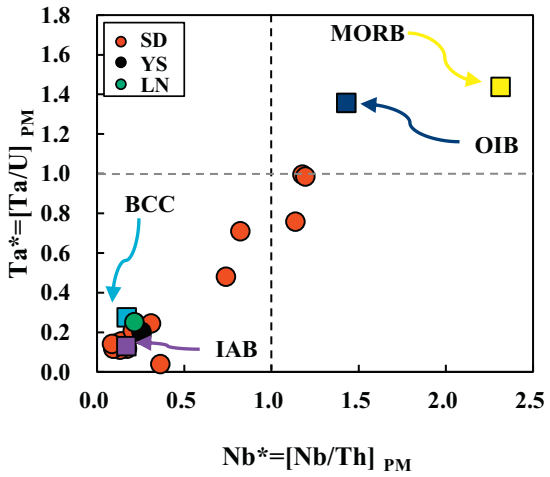

Fig. 10. Diagram of Ta* vs. Nb* for the dykes (after Niu and Batiza, 1997). Compared with common basalts, the dikes have Ta and Nb deficiencies, resembling continental crust and IAB. Data of primitive mantle and average oceanic basalts (OIB, N-MORB) are from Sun and McDonough (1989). BCC composition is from Rudnick and Gao (2003). LN-dykes in Liaoning, YS-dykes in Yanshan, SD-dykes in Shandong.

5. Discussion

5.1. Crust contamination vs. source enrichment

On MgO variation diagrams (Fig. 6), all samples form a scattered negative trend in SiO_2-MgO plot and scattered positive trends in CaO/Al_2O_3-MgO, Cr-MgO and Ni-MgO plots, which are consistent, to a first-order, with varying extent of fractional crystallization dominated by olivine and clinopyroxene as the major liquidus phases. The lack of correlations of MgO vs. Fe_2O_3 and MgO vs. TiO_2 disapprove fractionation of Fe–Ti oxides.

Crustal contamination or magma mixing as possible processes may affect the compositions of erupted basaltic melts (e.g., the mafic dykes we study here) and need to be evaluated before discussing mantle sources and processes. To evaluate these processes is not straightforward here because the dykes we studied have "crust-like" or "arc-like" geochemical features, e.g., negative Nb-Ta-Ti and positive Pb anomalies, high initial $^{87}Sr/^{86}Sr$ and low $\varepsilon_{Nd}(t)$ and $\varepsilon_{Hf}(t)$ values. Nevertheless, we show below that these dykes may had experienced limited crustal contamination.

The continental crust is characterized by elevated abundances of SiO_2 of 61.8 wt% (on average) and large ion lithophile elements (LILEs), yet relatively depleted high field strength elements (HFSEs) (Rudnick and Gao, 2003) with high $^{87}Sr/^{86}Sr$, low $^{143}Nd/^{144}Nd$ and low $^{176}Hf/^{177}Hf$. Also, given the relative incompatibility of $D_{Nb} \approx D_{Th} < D_{Ta} \approx D_U$ during basaltic magmatism (Niu and Batiza, 1997; Niu and O'Hara, 2009), the dykes show Ta* and Nb* closely resemble those of the BCC and IAB, but significantly differ from the MORB and OIB, suggesting the effect of possible crustal contamination (Fig. 10). However, the poor correlations between SiO_2 (except the two samples of SiO_2 > 60 wt%) and $\varepsilon_{Nd}(t)$, $\varepsilon_{Hf}(t)$ and $(^{206}Pb/^{204}Pb)_i$ (Fig. 11) indicate that crustal contamination, if any, is insignificant. Thus, the apparently contradictory implications (Figs. 10 and 11) requires an open-minded consideration. Additionally, the mafic dykes display high concentrations of Sr (501–1569 ppm) and Ba (507–2326 ppm) that are much higher than the crustal values of the BCC (Sr = 320 ppm; Ba = 456 ppm; Rudnick

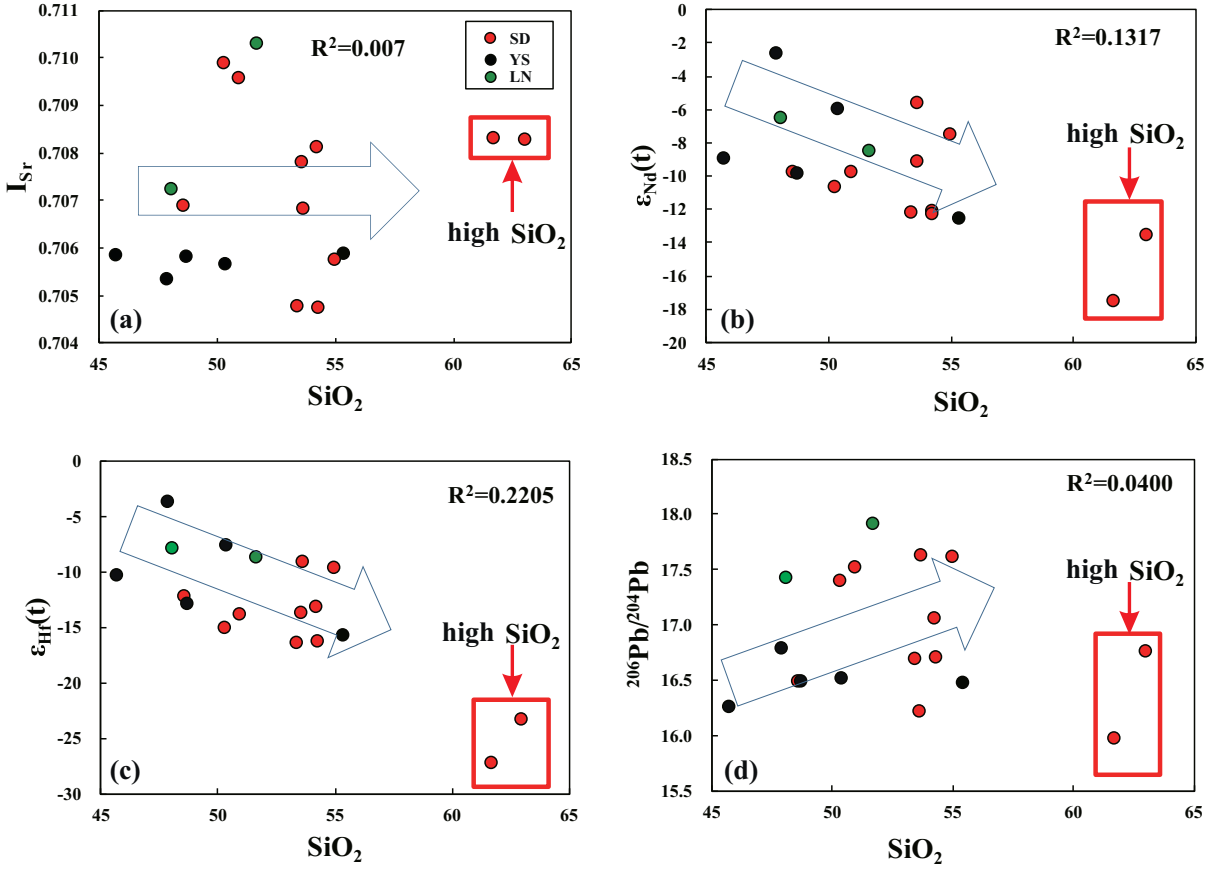

Fig. 11. (a) $(^{87}Sr/^{86}Sr)_i$, (b) $\varepsilon_{Nd}(t)$, (c) $\varepsilon_{Hf}(t)$ and (d) $(^{206}Pb/^{204}Pb)_i$ vs. SiO_2 diagrams of the Cretaceous dykes from the eastern China. The poor correlations between SiO_2 and $(^{87}Sr/^{86}Sr)_i$, $\varepsilon_{Nd}(t)$, $\varepsilon_{Hf}(t)$ as well as $(^{206}Pb/^{204}Pb)_i$ clearly imply that there was little to no crustal contamination during the ascent of magmas. LN-dykes in Liaoning, YS-dykes in Yanshan, SD-dykes in Shandong.

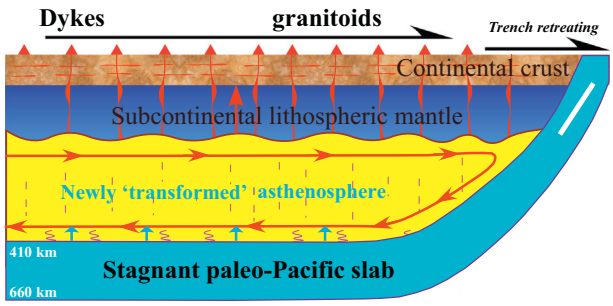

Fig. 12. A possible model showing the generation of dykes in eastern China (modified from Niu et al., 2015). The stagnant Pacific plate in the mantle transition zone (410–660 km) experiences isobaric heating and dehydration with time (Niu, 2005; Niu et al., 2015). The water so released reduces both the viscosity and density of the asthenospheric mantle above, forming hydrous melts. The latter, when rising at the base of the lithosphere, further hydrates the lithosphere and "converts" the basal portions into convective asthenosphere while producing our enriched basaltic melts with $\varepsilon_{Nd} < 0$, $\varepsilon_{Hf} < 0$. Hence, the lithospheric thinning and enriched Mesozoic basaltic volcanism are both the response to the hydration of the basal lithosphere with the water ultimately derived from "ancient" subducted oceanic lithosphere (slabs) lying within the transition zone.

and Gao, 2003) and hence these data exclude crustal assimilation to have played a significant role in the petrogenesis. The negative Nb* and Ta* anomalies observed in Fig. 10 must have been inherited from sources or source histories.

5.2. Modification of the mantle source by subducted components

The lithospheric mantle is cold and isotopically enriched with high $^{87}Sr/^{86}Sr_i$ and low $\varepsilon_{Nd}(t)$ and $\varepsilon_{Hf}(t)$ because of its low-degree melt metasomatism history and long-time isolation from the convective mantle. Relatively high $^{87}Sr/^{86}Sr$ (0.7048 to 0.7103) and $^{206}Pb/^{204}Pb$ (18.79–18.85) and low $\varepsilon_{Nd}(t)$ (−12.3 to −5.7) and $\varepsilon_{Hf}(t)$ (−16.5 to −8.0) of these dykes are consistent with their derivation from the ancient fertile lithospheric mantle. Meanwhile, the arc-like elemental signatures of these dykes, including the enrichment in LREEs and LILEs and depletion in HFSEs (negative Nb, Ta, Zr, Hf and P anomalies) could be explained by two possible petrogenetic models: (1) an enriched mantle domain metasomatized by a fluid from subducted plate (Huang et al., 2012; Liang et al., 2017, 2018); (2) mantle source region contaminated by recycled continental crust materials (Ma et al., 2016). As crustal contamination was not an important process during emplacement of the dykes (see above), the spatial geochemical variations shown in Figs. 8, 9, 11 primarily represent a real variation of the ratios for the source mantle. In addition, all these dykes plot along the mantle array in the Hf–Nd isotopic space (Fig. 8 b), suggesting that the mantle source isotopic variation is largely controlled by simple magmatic processes.

Ayers (1998) suggested that subduction-zone hydrous fluids have significantly low Nb/U ratio, which was ascribed to the transfer of significant amounts of LILE but not HFSE into the slab-derived hydrous fluid. The HFSEs are more likely to be stored in residual rutile and ilmenite that persist in the subducted slab (Ryerson and Watson, 1987) while fluid-mobile incompatible trace elements are lost during the dehydration. Thus, fluids produced at the sub-arc depths would be characterized by enrichment in fluid-mobile incompatible trace elements such as LILE and Pb but depletion in HFSE such as Nb and Ta (Ringwood, 1990; Zheng et al., 2006; Xu et al., 2013). The relative Nb-Ta-Ti depletion in the Mesozoic dykes cannot be interpreted as the presence of rutile as a residual phase because (1) the rutile residue requires the source rock to be basaltic (e.g., eclogite); (2) partial melting of eclogites cannot produce basaltic melts we studied here; (3) rutile has very high solubility in silicate melt and cannot exist as a residual phase during basalt melting (Ryerson and Watson, 1987). Hence, fluid-related metasomatism cannot explain the isotopic enrichment.

Beneath eastern continental China, the subducted paleo-Pacific plate, which can release water as a result of thermal equilibrium with the ambient mantle (Niu, 2005, 2014), has been detected to lie horizontally in the mantle transition zone (410–660 km) in Cenozoic (Kárason and van der Hilst, 2000; Zhao et al., 2004). It should be noted that the effect of transition-zone slab dehydration differs from subduction-zone metamorphic dehydration in triggering arc magmatism. The transition-zone dehydration is a magmatic process producing hydrous melt that rises and weakens the base of the lithosphere (Niu, 2005).

The mantle metasomatism has been widely used to explain the geochemically enriched signatures of the cratonic lithospheric mantle (e.g., Hawkesworth et al., 1990; Lloyd and Bailey, 1975). For example, mantle metasomatism might explain the large negative $\varepsilon_{Nd}(t)$ and $\varepsilon_{Hf}(t)$ values of the mafic dykes. While the sub-continental mantle lithosphere (SCLM) which were subjected to previous melt extraction is likely depleted in major elements (i.e., high $Mg^{\#}$, low Al_2O_3 and high CaO/Al_2O_3), it can be re-enriched in terms of incompatible elements throughout its long histories via mantle metasomatism (e.g., O'Reilly and Griffin, 1988), similar to the processes taking place at the lithosphere-asthenosphere boundary beneath ocean basins (Niu and Green, 2018; Niu and O'Hara, 2003) or in a mantle wedge environment (Donnelly et al., 2004). The metasomatism would not significantly affect the major elements, but may result in enrichments in volatiles and the more incompatible elements, leading to enriched isotopic signatures (e.g., the elevated ratios of Rb/Sr, U/Pb, Th/Pb, Nd/Sm and Hf/Lu, radiogenic Sr, Pb isotopes and unradiogenic Nd, Hf isotopes; Niu, 2005). Hence, the mantle metasomatism can explain the isotopically enriched signatures in the mafic dykes (i.e., high $^{87}Sr/^{86}Sr$, low ε_{Nd} and ε_{Hf}).

Niu (2005, 2014) suggested that the water released from the subducted oceanic lithosphere in the mantle transition zone (410–660 Km) beneath eastern China will rise in the form of hydrous melt through the upper asthenospheric mantle and reach the lithosphere. Following these interpretations, we propose that the dykes in eastern continental China were derived from partial melting of the sub-continental lithospheric mantle (SCLM) refertilized by slab derived fluids in the form of hydrous melt, which are consistent with our data.

5.3. Geodynamic implications

The rapid delamination, thermal erosion and flat subduction models for interpreting the NCC destructions since the Mesozoic are physically problematic (Niu et al., 2015). There are many lines of evidence suggest that the presence of the similar transition zone slab back in the Mesozoic as indicated by the widespread Cretaceous magmas throughout eastern China from NE to SE, which marks the presence of an active continental margins related to northwestward subduction of the paleo-Pacific seafloor (Niu, 2014; Niu et al., 2015). The subducted Pacific slab beneath eastern China is shown to be stagnant in the mantle transition zone on tomographic image (Huang et al., 2012). This transition zone dehydration process will facilitate the production of hydrous melt that ascends and migrates upwards to weaken the base of the ancient lithosphere by hydration, which can effectively convert the basal lithospheric mantle into the asthenospheric mantle. This is in effect the process of lithosphere thinning (Niu, 2005), accompanied by the surface volcanism with the ascending hydrous melt assimilated with the metasomatic components in the prior lithosphere to form geochemically enriched basaltic melts (Niu, 2005), i.e., the mafic melts in eastern continental China of our study. To be specific, recent studies revealed that the lithospheric mantle beneath the NCC was more hydrous (>1000 ppm) at ~125 Ma, which is significantly higher than H_2O contents of the lithospheric mantle in the Late Cretaceous and the Cenozoic (Li et al., 2015). Therefore, we suggest that the slab-derived hydrous fluid in the form of hydrous melt from the subducted paleo-Pacific plate triggered the partial melting of the metasomatized mantle and resulted in the magmatism in eastern continental China (Kuritani et al., 2011; Sakuyama et al., 2013). Previous subduction-induced trace element enrichment may also exist, but it might be overprinted or intensively modified by such a westward subduction event. The slab-

derived water in the form of incipient hydrous melt percolates upwards, metasomatizes the upper mantle, and weakens/converts the basal lithosphere into asthenosphere accompanied by melting of the being converted lithosphere/asthenosphere to produce voluminous mafic magmas (Fig. 12). Mesozoic lithosphere thinning in eastern continental China is best explained by a process that "transformed" the basal portion of the lithosphere into convective asthenosphere by hydration. The Mesozoic volcanism (mafic magmas) may be genetically associated with the lithospheric thinning because the basaltic source is ancient isotopically enriched ($\varepsilon_{Nd} < 0$, $\varepsilon_{Hf} < 0$) lithosphere which had been converted into asthenosphere with the melts undergoing crystallization to evolve into some of the more felsic dykes. This mafic magmas underplated the lower crust, causing partial melting to generate the widespread granitoids throughout eastern continental China in the Cretaceous.

6. Conclusions

(1) The K–Ar and zircon ages indicate that the dykes from eastern continental China we study are of Early Cretaceous age (130-110 Ma), broadly synchronous with the massive emplacement of granitic plutons in the region, ultimately as the consequence of lithosphere thinning.
(2) The dykes have arc-like magmatic characteristics with enrichment in LILEs and LREEs, high $(^{87}Sr/^{88}Sr)_i$, low $\varepsilon_{Nd}(t)$ and the $\varepsilon_{Hf}(t)$, pointing to their parental magma derivation from geochemically enriched mantle lithosphere. During ascent, these magmas underwent fractional crystallization of olivine and clinopyroxene with limited crustal contamination.
(3) The geochemical enrichment of the mantle lithosphere as the source of magmas parental to these dykes resulted from ancient metasomatism most likely caused by water (hydrous melt) released from the subduction of the paleo-Pacific slab in the mantle transition zone or even earlier events.
(4) The basaltic melts rise, underplate/intrude the lower crust en route to the surface (the Mesozoic basalts/ minor andesites with "arc" signature), and cause crustal melting for the observed granitoid magmatism in eastern continental China. In fact, the widespread Mesozoic granitoids in eastern continental China all resulted from crustal melting induced by mantle derived melts, ultimately associated with the lithosphere thinning.

Acknowledgments

We thank Huixia Cui, Yan Hu for sample preparation. We thank Jianxin Zhao for laboratory assistance in geochemistry and isotope analysis. We appreciate two anonymous reviewers for constructive comments and editor Dr. Andrew Kerr for handing this manuscript. This work was supported by grants from Chinese Academy of Sciences, regional and local authorities (Shandong Province and City of Qingdao, U1606401), Qingdao National laboratory of ocean sciences and Technology (2015ASKJ03) and National Natural Science Foundation of China (41630968, 91014003) and the 111 Project of China (B118048).

Appendix A. Supplementary data

Supplementary data to this article can be found online at https://doi.org/10.1016/j.lithos.2019.02.024.

References

Ayers, J., 1998. Trace element modeling of aqueous fluid-peridotite interaction in the mantle wedge of subduction zones. Contributions to Mineralogy and Petrology 132, 390–404.
Barry, T.L., Kent, R.W., 1988. Cenozoic magmatism in Mongolia and the origin of central and East Asian basalts. In: Chung, M.F.J., Lo, S.L., Lee, C.H., Kent, T.Y. (Eds.), Mantle Dynamics and Plate Interactions in East Asia. vol. 27, pp. 347–364 American Geophysical Union-Geodynamics Series.
Belousova, E., Griffin, W., O'Reilly, S.Y., Fisher, N., 2002. Igneous zircon: trace element composition as an indicator of source rock type. Contributions to Mineralogy and Petrology 143, 602–622.
Chen, S., Wang, X., Niu, Y., Sun, P., Duan, M., Xiao, Y., Xue, Q., 2017. Simple and cost-effective methods for precise analysis of trace element abundances in geological materials with ICP-MS. Science Bulletin 62 (4), 277–289.
Dai, L.Q., Zheng, Y.F., Zhao, Z.F., 2016. Termination time of peak decratonization in North China: geochemical evidence from mafic igneous rocks. Lithos 240–243, 327–336.
Deng, J.F., Su, S.G., Niu, Y.L., Liu, C., Zhao, G.C., Zhao, X.G., Zhou, S., Wu, Z.X., 2007. A possible model for the lithospheric thinning of North China Craton: evidence from the Yanshanian (Jura-cretaceous) magmatism and tectonic deformation. Lithos 96, 22–35.
Donnelly, K.E., Goldstein, S.L., Langmuir, C.H., Spiegelman, M., 2004. Origin of enriched ocean ridge basalts and implications for mantle dynamics. Earth and Planetary Science Letters 226, 347–366.
Dupuy, C., Liotard, J.M., Dostal, J., 1992. Zr/Hf fractionation in intraplate basaltic rocks: carbonate metasomatism in the mantle source. Geochimica et Cosmochimica Acta 56 (6), 2417–2423.
Fan, W.M., Menzies, M.A., 1992. Destruction of aged lower lithosphere and accretion of asthenosphere mantle beneath eastern China. Geotectonica et Metallogenia 16, 171–180.
Gao, S., Rudnick, R.L., Carlson, R.W., McDonough, W.F., Liu, Y.S., 2002. *Re*–Os evidence for replacement of ancient mantle lithosphere beneath the North China Craton. Earth Planet Science Letters 198, 307–322.
Gao, S., Rudnick, R.L., Yuan, H.L., Liu, X.M., Liu, Y.S., Xu, W.L., Ling, W.L., Ayers, J., Wang, X.C., Wang, Q.H., 2004. Recycling lower continental crust in the North China craton. Nature 432, 892–897.
Griffin, W.L., Zhang, A.D., O'Reilly, S.Y., Ryan, C.G., 1998. Phanerozoic evolution of the lithosphere beneath the Sino-Korean craton. In: Flower, M.F.J., Chung, S.L., Lo, C.H., Lee, T.Y. (Eds.), Mantle Dynamics and Plate Interactions in East Asia. 27, pp. 107–126 American Geophysical Union Geodynamics Series.
Guo, P.Y., Niu, Y.L., Ye, L., Liu, J.J., Sun, P., Cui, H.X., Zhang, Y., Gao, J.P., Su, L., Zhao, J.X., Feng, Y.X., 2014. Lithosphere thinning beneath west North China Craton: evidence from geochemical and Sr-Nd-Hf isotope compositions of Jining basalts. Lithos 202–203, 37–54.
Hart, S.R., 1984. A large-scale isotope anomaly in the Southern Hemisphere mantle. Nature 309, 753–757.
Hawkesworth, C.J., Erlank, A.J., Kempton, P.D., Waters, F.G., 1990. Mantle metasomatism: isotope and trace-element trends in xenoliths from kimberley, south africa. Chemical Geology 85 (1), 19–34.
Hong, D., Niu, Y.L., Xiao, Y.Y., Sun, P., Kong, J.J., Guo, P.Y., Shao, F.L., Wang, X.H., Duan, M., Xue, Q.Q., Gong, H.M., Chen, S., 2018. Origin of the Jurassic-Cretaceous intraplate granitoids in Eastern China as a consequence of paleo-Pacific plate subduction. Lithos 322, 405–419.
Hoskin, P.W.O., Schaltegger, U., 2003. The Composition of Zircon and Igneous and Metamorphic Petrogenesis. Mineralogical Society of America, Washington, DC, pp. 36 ETATS–UNIS.
Huang, X.L., Zhong, J.W., Xu, Y.G., 2012. Two tales of the continental lithospheric mantle prior to the destruction of the North China Craton: insights from Early Cretaceous mafic intrusions in western Shandong, east China. Geochimica et Cosmochimica Acta 96, 193–214.
Jahn, B.M., Wu, F.Y., Chen, B., 2000a. Granitoids of the Central Asian orogenic belt and continental growth in the Phanerozoic. Transactions of the Royal Society of Edinburgh, Earth Science 91, 181–193.
Jahn, B.M., Wu, F.Y., Chen, B., 2000b. Massive granitoid generation in Central Asia: Nd isotope evidence and implication for continental growth in the Phanerozoic. Episodes 23 (2), 82–92.
Jahn, B.M., Capdevila, R., Liu, D.Y., Vernon, A., Badarch, G., 2004. Sources of Phanerozoic granitoids in the transect Bayanhongor–Ulaan Baatar, Mongolia: geochemical and Nd isotopic evidence, and implications for Phanerozoic crustal growth. Journal of Asian Earth Sciences 23 (5), 629–653.
Kárason, H.., van der Hilst, R., 2000. Constraints on mantle convection from seismic tomography. Geophys.Monogr. 121, 277–288.
Kuritani, T., Ohtani, E., Kimura, J.I., 2011. Intensive hydration of the mantle transition zone beneath China caused by ancient slab stagnation. Nature Geoscience 4 (10), 713–716.
Lloyd, F.E., Bailey, D., 1975. Light element metasomatism of the continental mantle: theevidence and the consequences. Phys. Chem. Earth 9, 389–416.
Li, S.Z., Zhao, G.C., Dai, L.M., Liu, X., Zhou, L.H., Santosh, M., Suo, Y.H., 2012. Mesozoic basins in eastern China and their bearing on the deconstruction of the North China Craton. Journal of Asian Earth Sciences 47, 64–79.
Li, S., Wang, T., Wilde, S.A., Tong, Y., 2013. Evolution, source and tectonic significance of early Mesozoic granitoid magmatism in the central Asian orogenic belt (central segment). Earth-Science Reviews 126 (11), 206–234.
Li, P., Xia, Q.K., Deloule, E., Chen, H., Gu, X.Y., Feng, M., 2015. Temporal variation of H_2O content in the lithospheric mantle beneath the eastern North China Craton: implications for the destruction of cratons. Gondwana Research 28, 276–287.
Liang, Y., Liu, X., Qin, C., Li, Y., Chen, J., Jiang, J., 2016. Petrogenesis of early cretaceous mafic dikes in southeastern jiaolai basin, jiaodong peninsula, china. International Geology Review 1–20.
Liang, Y.Y., Liu, X.F., Qin, C., Li, Y., Chen, J., Jiang, J.Y., 2017. Petrogenesis of Early Cretaceous mafic dikes in southeastern Jiaolai basin, Jiaodong Peninsula, China. International Geology Review 59, 131–150.

Liang, Y., Deng, J., Liu, X., Wang, Q., Qin, C., Li, Y., 2018. Major and trace element, and sr isotope compositions of clinopyroxene phenocrysts in mafic dykes on jiaodong peninsula, southeastern north china craton: insights into magma mixing and source metasomatism. Lithos 302–303.
Lin, W., Wang, Q.C., 2006. Late Mesozoic extensional tectonics in the North China block: a crustal response to subcontinental mantle removal? Bulletin de la Societe Geologique de France 177, 287–297.
Liu, D.Y., Nutman, A.P., Compston, W., Wu, J., She, Q., 1992. Remnants of N3800 Ma crust in the Chinese part of the Sino-Korean Craton. Geology 20, 339–342.
Liu, J.L., Davis, G.A., Ji, M., Guan, H.M., Bai, X.D., 2008a. Crustal detachment and destruction of the Keel of North China Craton: constraints from Late Mesozoic extensional structures. Earth Science Frontiers 15, 72–81.
Liu, S., Hu, R., Gao, S., Feng, C., Qi, Y., Wang, T., Feng, G., Coulson, I.M., 2008b. U–Pb zircon age, geochemical and Sr-Nd-Pb-Hf isotopic constraints on age and origin of alkaline intrusions and associated mafic dikes from Sulu orogenic belt, Eastern China. Lithos 106, 365–379.
Liu, Y.S., Gao, S., Hu, Z.C., Gao, C.G., Zong, K.Q., W ang, D.B., 2010a. Continental and oceanic crust recycling-induced melt-peridotite interactions in the Trans-North China Orogen: U–Pb dating, Hf isotopes and trace elements in zircons from mantle xenoliths. Journal of Petrology 51, 537–571.
Liu, Y.S., Hu, Z.C., Zong, K.Q., Gao, C.G., Gao, S., Xu, J., Chen, H.H., 2010b. Reappraisement and refinement of zircon U–Pb isotope and trace element analyses by LA-ICP-MS. Chinese Science Bulletin 55, 1535–1546.
Ludwig, K., 2012. User's Manual for Isoplot Version 3.75–4.15: A Geochronological Toolkit for Microsoft. Excel Berkley Geochronological Center Special Publication (No. 5).
Ma, L., Jiang, S.Y., Hofmann, A.W., Xu, Y.G., Dai, B.Z., Hou, M.L., 2016. Rapid lithospheric thinning of the north china craton: new evidence from cretaceous mafic dikes in the jiaodong peninsula. Chemical Geology 432, 1–15.
Menzies, M.A., Fan, W.M., Zhang, M., 1993. Paleozoic and Cenozoic lithoprobe and the loss of >120 km of Archean lithosphere, Sino-Korean craton, China. In: Prichard, H.M., Alabaster, T., Harris, N.B.W., Neary, C.R. (Eds.), Magmatic Processes and Plate Tectonic. vol. 76. Geological Society Special Publication, pp. 71–81.
Míková, J., Denková, P., 2007. Modified chromatographic separation scheme for Sr and Nd isotope analysis in geological silicate samples. Journal of Geosciences 52, 221–226.
Niu, Y., 2005. Generation and evolution of basaltic magmas: some basic concepts and a new view on the origin of Mesozoic-Cenozoic basaltic volcanism in eastern China. Geological Journal of China Universities 11, 9–46 (in English with Chinese abstract).
Niu, Y.L., 2014. Geological understanding of plate tectonics: Basic concepts, illustrations, examples and new perspectives. Global Tectonics and Metallogeny 10, 23–46.
Niu, Y.L., Green, D.H., 2018. The petrological control on the lithosphere-asthenosphere boundary (LAB) beneath ocean basins. Earth-Science Reviews 185, 301–307.
Niu, Y.L., O'Hara, M.J., 2003. Origin of ocean island basalts: a new perspective from petrology, geochemistry and mineral physics considerations. Journal of Geophysical Research 108 ECV5 1-19.
Niu, Y.L., O'Hara, M.J., 2009. MORB mantle hosts the missing Eu (Sr, Nb, Ta and Ti) in the continental crust: new perspectives on crustal growth, crust-mantle differentiation and chemical structure of oceanic upper mantle. Lithos 112, 1–17.
Niu, L., Batiza, R., 1997. Trace element evidence from seamounts for recycled oceanic crust in the Eastern Pacific mantle. Earth and Planetary Science Letters 148, 471–483.
Niu, Y., Liu, Y., Xue, Q., Shao, F., Chen, S., Duan, M., Kong, J., ... Zhang, Yu, 2015. Exotic origin of the Chinese continental shelf: new insights into the tectonic evolution of the western Pacific and eastern China since the Mesozoic. Science Bulletin 60 (18), 1598–1616.
O'Reilly, S.Y., Griffin, W.L., 1988. Mantle metasomatism beneath western Victoria, Australia, part I, metasomatic processes in Cr-diopside lherzolites. Geochimica et Cosmochimica Acta 52, 433–447.
Ringwood, A.E., 1990. Slab-mantle interactions: Petrogenesis of intraplate magmas and structure of the upper mantle. Chemical Geology 82, 187–207.
Rudnick, R.L., Gao, S., 2003. Composition of the continental crust. Treatise on Geochemistry 3, 1–64.
Ryerson, F.J., Watson, E.B., 1987. Rutile saturation in magmas: implications for Ti-Nb-Ta depletion in island-arc basalts. Earth and Planetary Science Letters 86, 225–239.
Sakuyama, T., Tian, W., Kimura, J.I., Fukao, Y., Hirahara, Y., Takahashi, T., Senda, R., Chang, Q., Miyazaki, T., Obayashi, M., Kawabata, H., Tasumi, Y., 2013. Melting of dehydrated oceanic crust from the stagnant slab and of the hydrated mantle transition zone: constraints from Cenozoic alkaline basalts in eastern China. Chemical Geology 359, 32–48.
Sang, H.Q., Wang, F., He, H.Y., Wang, Y.L., Yang, L.K., Zhu, R.X., 2006. Intercalibration of ZBH-25 biotite reference material utilized for K–Ar and 40Ar–39Ar age determination. Acta Petrologica Sinica 22 (12), 3059–3078.
Sun, S.-s., McDonough, W.F., 1989. Chemical and isotopic systematics of oceanic basalts: implications for mantle composition and processes. Geological Society, London, Special Publications 42, 313–345.
Vervoort, J.D., Blichert-Toft, J., 1999. Evolution of the depleted mantle: Hf isotope evidence from juvenile rocks through time. Geochimica et Cosmochimica Acta 63 (3/4), 533–556.
Wang, X.C., Wilde, S.A., Li, Q.L., 2015. Continental flood basalts derived from the hydrous mantle transition zone. Nature Communications 6.
Windley, B.F., Alexeiev, D., Xiao, W., Kröner, A., Badarch, G., 2007. Tectonic models for accretion of the Central Asian Orogenic Belt. Journal of the Geological Society of London 164, 31–47.
Windley, B.F., Maruyama, S., Xiao, W.J., 2010. Delamination/thinning of sub-continental lithospheric mantle under eastern China; the role of water multiple subduction. American Journal of Science 310, 1250–1293.
Wong, W.H., 1929. The Mesozoic orogenic movement in Eastern China. Bulletin of the Geological Society of China 8, 33–44.
Wu, F.Y., Ge, W.C., Sun, D.Y., Guo, C.L., 2003. Discussions on the lithospheric thinning in eastern China. Earth Science Frontiers 10, 51–60 (in Chinese with English abstract).
Wu, F.Y., Lin, J.Q., Wilde, S.A., Zhang, X.O., Yang, J.H., 2005. Nature and significance of the Early Cretaceous giant igneous event in eastern China. Earth and Planetary Science Letters 233, 103–119.
Wu, K., Ling, M.X., Sun, W., Guo, J., Zhang, C.C., 2017. Major transition of continental basalts in the early cretaceous: implications for the destruction of the north china craton. Chemical Geology 470.
Xie, Z., Li, Q.Z., Gao, T.S., 2006. Comment on "Petrogenesis of post-orogenic syenites in the Sulu orogenic belt, east China: geochronological, geochemical and Nd-Sr isotopic evidence" by Yang et al. Chemical Geology 235, 191–194.
Xu, Y.G., 2014. Recycled oceanic crust in the source of 90-40 Ma basalts in North and Northeast China: evidence, provenance and significance. Geochimica et Cosmochimica Acta 143, 49–67.
Xu, Y.G., Ma, J.L., Huang, X.L., Iizuka, Y., Chung, S.L., Wang, Y.B., Wu, X.Y., 2004. Early Cretaceous gabbroic complex from Yinan, Shandong Province: petrogenesis and mantle domains beneath the North China Craton. International Journal of Earth Sciences 93, 1025–1041.
Xu, Y.G., Blusztajn, J., Ma, J.L., Suzuki, K., Liu, J.F., Hart, S.R., 2008. Late Archean to early Proterozoic lithospheric mantle beneath the western North China craton: Sr-Nd-Os isotopes of peridotite xenoliths from Yangyuan and Fansi. Lithos 102, 25–42.
Xu, Y.G., Li, H.Y., Pang, C.J., He, B., 2009. On the timing and duration of the destruction of the North China Craton. Chinese Science Bulletin 54, 3379–3396.
Xu, Y.G., Zhang, H.H., Qiu, H.N., Ge, W.C., Wu, F.Y., 2012. Oceanic crust components in continental basalts from Shuangliao, Northeast China: derived from the mantle transition zone? Chemical Geology 328, 168–184.
Xu, W.L., Pei, F.P., Wang, F., Meng, E., Ji, W.Q., Yang, D.B., Wang, W., 2013. Spatial-temporal relationships of Mesozoic volcanic rocks in NE China: constraints on tectonic overprinting and transformations between multiple tectonic regimes. Journal of Asian Earth Sciences 74, 167–193.
Yang, J.H., Wu, F.Y., Wilde, S.A., 2003. A review of the geodynamic setting of largescale Late Mesozoic gold mineralization in the North China Craton: an association with lithospheric thinning. Ore Geol. Rev. 23, 125–152.
Yang, Y.H., Zhang, H.F., Chu, Z.Y., Xie, L.W., Wu, F.Y., 2010. Combined chemical separation of Lu, Hf, Rb, Sr, Sm and Nd from a single rock digest and precise and accurate isotope determinations of Lu–Hf, Rb–Sr and Sm–Nd isotope systems using Multi-Collector ICP-MS and TIMS. International Journal of Mass Spectrometry 290, 120–126.
Zhang, H.F., Sun, M., Zhou, M.F., Fan, W.M., Zhou, X.H., Zhai, M.G., 2004. Highly heterogeneous late Mesozoic lithospheric mantle beneath the North China Craton: evidence from Sr-Nd-Pb isotopic systematics of mafic igneous rocks. Geological Magazine 141, 55–62.
Zhao, G.C., Wilde, S.A., Cawood, P.A., Sun, M., 2001. Archean blocks and their boundaries in the North China Craton: lithological, geochemical, structural and P-T path constraints and tectonic evolution. Precambrian Research 107, 45–73.
Zhao, D., Lei, J., Tang, R., 2004. Origin of the Changbai intraplate volcano in Northeast China: Evidence fromseismic tomography. Chinese Sci. Bull 49, 1401–1408.
Zheng, J.P., O'Reilly, S.Y., Griffin, W.L., Lu, F.X., Zhang, M., 1998. Nature and evolution of Cenozoic lithospheric mantle beneath Shandong peninsula, Sino-Korean craton, eastern China. International Geology Review 40, 471–499.
Zheng, J.P., Griffin, W.L., O'Reilly, S.Y., Yang, J.S., Li, T.F., Zhang, M., Zhang, R.Y., Liou, J.G., 2006. Mineral chemistry of peridotites from Paleozoic, Mesozoic and Cenozoic lithosphere: constraints on mantle evolution beneath eastern China. Journal of Petrology 47, 2233–2256.
Zheng, J.P., Griffin, W.L., O'Reilly, S.Y., Yu, C.M., Zhang, H.F., Pearson, N., Zhang, M., 2007. Mechanism and timing of lithospheric modification and replacement beneath the eastern North China Craton: peridotitic xenoliths from the 100 Ma Fuxin basalts and a regional synthesis. Geochimica et Cosmochimica Acta 71, 5203–5225.
Zhou, X.M., Li, W.X., 2000. Origin of Late Mesozoic igneous rocks in Southeastern China: implications for lithosphere subduction and underplating of mafic magmas. Tectonophysics 326, 269–287.
Zhou, X.-H., Sun, M., Zhang, G.-H., Chen, S.-H., 2002. Continental crust and lithospheric mantle interaction beneath North China: isotopic evidence from granulite xenoliths in Hannuoba. Lithos 62, 111–124 Sino-Korean craton.
Zhu, R.X., Xu, Y.G., Zhu, G., Zhang, H.F., Xia, Q.K., Zheng, T.Y., 2012. Destruction of the North China Craton. Science China Earth Sciences 55, 1565–1587.
Zou, H.B., Zindler, A., Xu, X.S., Qi, Q., 2000. Major, trace element, and Nd, Sr and Pb isotope studies of Cenozoic basalts in SE China: mantle sources, regional variations, and tectonic significance. Chemical Geology 171, 33–47.